2017 IEEE International Conference on Robotics and Automation (ICRA)
Singapore, May 29 - June 3, 2017

Path following for a biomimetic underwater vehicle based on ADRC

Rui Wang, Shuo Wang, Yu Wang, and Chong Tang

Abstract— **This paper addresses the problem of path following for a biomimetic underwater vehicle (BUV) propelled by undulatory fins with uncertain model and unknown disturbance. The mechanical structure of the BUV is briefly described. Moreover, the general kinematics and dynamics models of the vehicle are presented and the path following problem is formulated. The controller combining line-of-sight (LOS) guidance system with active disturbance rejection control (ADRC) technique is designed to maneuver the BUV to follow a predefined parameterized curve. Specifically, a guidance system based on LOS principle is implemented to decouple the multi-variable system to steer the surge speed and the course respectively. Furthermore, in order to deal with model uncertainty, ADRC is used in development of the surge speed controller and the course controller. Finally, simulations and experimental results validated the performance of the proposed path following control scheme.**

I. INTRODUCTION

Various underwater vehicles have been developed for ocean exploration and intervention as they make it possible to go far beneath the ocean surface, investigate aquatic biological systems, and furthermore perform intervention tasks [1]. However, as operations in dangerous and complex underwater environments become more common and complicated, the development of biomimetic underwater vehicle (BUV) propelled by undulatory fins has drawn extensive attention, whose appealing nature involves stronger disturbance rejection, higher propulsive efficiency, more excellent maneuverability, and quieter actuation than conventional marine vehicles powered by rotary propellers [2].

Recently, growing research in propulsion and maneuvering mechanisms used by fish with fin propulsion has demonstrated a variety of prospective utilities in undersea vehicles, and some researchers have developed several kinds of BUVs propelled by undulatory fins [3]−[5]. Sfakiotakis *et al.* developed the earliest undulatory-fin device using the parallel bellows actuator in 2001 [3]. Hereafter, Northwestern University designed a bio-inspired robotic knifefish with an undulatory propulsor which used 32 servo motors to drive the long-fin [4]. Osaka University proposed a squid-like underwater robot with two undulating side fins mimicking stingrays or cuttlefishes [5]. However, to our knowledge, most of researchers focus on undulatory fin control, but seldom consider path following control, which is of primary importance for most applications, for those BUVs.

Remarkably, path following control for AUVs or surface ships has received great attention from worldwide researchers [6]−[9]. Do *et al.* developed a nonlinear robust adaptive control strategy to force an underactuated surface ship to follow a predefined path at a desired speed using Lyapunovs direct method [6]. Aguiar *et al.* addressed the problem of path-following control design for underactuated autonomous vehicles in the presence of large modeling parametric uncertainty using adaptive supervisory control that combines logic-based switching with Lyapunov-based techniques [7]. Breivik and Fossen proposed a guidance-based path following approach to follow straight lines and circles for fully actuated vessels [8]. Fredriksen *et al.* designed a line-of-sight (LOS) motivated control using the cascaded control theory to globally κ-exponentially stabilizes an underactuated ship in three degrees of freedom (DOF) [9].

Although all the above literatures have achieved satisfactory performance on path following control, most of existing controllers rely on precise mathematical models of the AUVs or vessels, which are usually difficult to obtain in practice, especially for BUVs propelled by undulatory fins. It is relevant to point out that only a few authors have applied the proposed path following methods in the actual systems, possibly due to the nonholonomic constraints of the vehicles and the complexity of underwater environment. Moreover, the propulsion modes of AUVs and surface vessels are quite different from that of BUVs with oscillating fin propulsion.

Motivated by the above considerations, this paper aims to develop a close-loop control law for a BUV propelled by undulatory fins to ensure path following in the underwater space. Specifically, a guidance system based on LOS principle is implemented to decouple the multi-variable system to steer the surge speed and the course respectively. Moreover, in order to deal with model uncertainty, active disturbance rejection control (ADRC) technique is used in development of the surge speed controller and the course controller. ADRC was initially proposed by Han [10] and then simplified to linear ADRC by Gao [11], which is not predicated on an accurate and detailed dynamic model of the plant and is extremely tolerant of uncertainties and simple to use.

In the remainder of this paper, Section II formulates the path following problem. Path following control scheme is elaborated in Sections III. Simulations and experimental results are further provided in section IV. Finally, the conclusion and perspectives are presented in Section V.

R. Wang and C. Tang are with the State Key Laboratory of Management and Control for Complex Systems, Institute of Automation, Chinese Academy of Sciences, Beijing 100190, China, and also with University of Chinese Academy of Sciences, Beijing 100049, China

S. Wang and Y. Wang are with the State Key Laboratory of Management and Control for Complex Systems, Institute of Automation, Chinese Academy of Sciences, Beijing 100190, China (corresponding author: Dr. Y. Wang, yu.wang@ia.ac.cn)

II. CONTROL PROBLEM FORMULATION

A. Modeling of the RobCutt-II

The BUV we consider in this paper is named RobCutt-II, which is a mechatronic system motivated by the unique undulatory propulsion mode of cuttlefish. Specially, the mechanical design of the RobCutt-II is based on modular concepts. As shown in Fig. 1, the RobCutt-II is composed of three modules, including a tube-like main body, a five degrees of freedom manipulator [12] and two symmetrically arranged propulsors with fins propulsion [13]. In particular, with the coordinated control of the propagating waves on bilateral fins, the biomimetic propulsor can produce propulsive force and moment simultaneously, such that the RobCutt-II can perform diversified locomotion patterns, including forward/backward swimming, diving/floating motion and turning maneuver with high mobility [14].

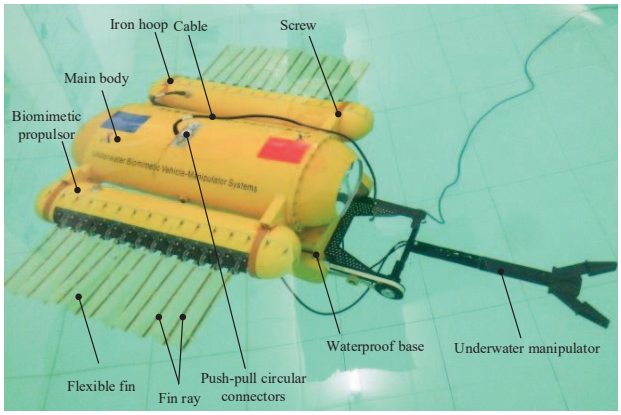

Fig. 1. RobCutt-II prototype.

In this paper, the path following issue is addressed in the horizontal plane. It should be noted that when swimming in the three-dimensional (3-D) underwater space, the RobCutt-II first dives or ascends to the desired depth using the method in [15] while maintaining horizontal position, then transits along the horizontal plane to the target. In addition, the RobCutt-II has good static stability due to large metacentric height, such that it's reasonable to neglect the motion in pitch and roll. It is further assumed that the nonlinear damping can be ignored since the linear damping is more significant than the nonlinear damping for underwater vehicle moving at low speed. Therefore, the three DOF kinematics and dynamics of the RobCutt-II can be represented as (see [16])

$$\begin{aligned} \dot{\eta} &= J(\psi)\nu \\ M\dot{\nu} &= -C(\nu)\nu - D\nu + \tau + \tau_d \end{aligned} \tag{1}$$

with

$$\begin{aligned} \eta &= [x\ y\ \psi]^{\mathrm{T}}, \\ \nu &= [u\ v\ r]^{\mathrm{T}}, \\ \tau &= [\tau_u\ 0\ \tau_r]^{\mathrm{T}}, \\ \tau_d &= [\tau_{du}\ \tau_{dv}\ \tau_{dr}]^{\mathrm{T}} \end{aligned}$$

where $\eta \in \mathbb{R}^3$ represents the earth-fixed position and course, $J(\psi) \in SO(3)$ is the rotational transform matrix from the earth-fixed reference frame to the vehicle-fixed reference frame, $\nu \in \mathbb{R}^3$ represents the vehicle-fixed velocities, M is the inertia matrix including hydrodynamic added inertia, $C(\nu)$ is the coriolis and centripetal matrix, D is the linear damping matrix, τ is vehicle-fixed propulsive force and moment, where τ_u, τ_r describe the propulsive force and moment acting on surge and yaw respectively, $\tau_d \in \mathbb{R}^3$ represents the disturbance forces or moment acting on surge, sway and yaw. In particular, bilateral symmetrical structure of the RobCutt-II implies that the matrixes M and D have the following structure based on the foregoing assumptions:

$$M \triangleq \begin{bmatrix} m_{11} & 0 & 0 \\ 0 & m_{22} & m_{23} \\ 0 & m_{23} & m_{33} \end{bmatrix} > 0, D \triangleq \begin{bmatrix} d_{11} & 0 & 0 \\ 0 & d_{22} & d_{23} \\ 0 & d_{32} & d_{33} \end{bmatrix}. \tag{2}$$

With the particular structure of the inertia matrix M given in (2), the coriolis and centripetal matrix $C(\nu)$ is parameterized as

$$C(\nu) \triangleq \begin{bmatrix} 0 & 0 & -m_{22}v - m_{23}r \\ 0 & 0 & m_{11}u \\ m_{22}v + m_{23}r & -m_{11}u & 0 \end{bmatrix}. \tag{3}$$

B. Problem Statement

In the path following task, the vehicle must reach and follow a reference path starting from the initial state. As depicted in Fig. 2, the initial position of the RobCutt-II is $p(x(t_0), y(t_0))$ in the inertial frame $O_E X_E Y_E$. $O_B X_B Y_B$ is the vehicle-fixed reference frame. The controller generates control signals τ_u and τ_r such that the barycenter of the RobCutt-II $p(x, y)$ globally follows a reference path Ω parameterized by $(x_d(s), y_d(s))$ with s being the arc length parameter at a desired surge speed u_d.

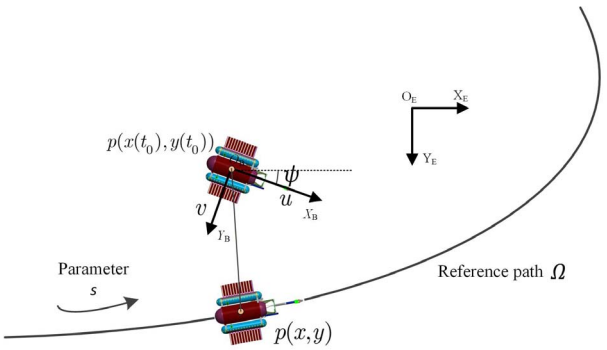

Fig. 2. Sketch map of path following for RobCutt-II.

III. PATH FOLLOWING CONTROL SCHEME

This section presents the control algorithm to solve the path following problem of the RobCutt-II. As show in Fig. 3, the path following controller is mainly composed of four parts. A guidance system based on LOS principle is firstly described in this section. Then the course controller and the surge speed controller based on ADRC technique are presented, respectively. Notice that the control signals of

the surge speed controller and course controller are propulsive force τ_u and moment τ_r respectively. However, the control parameters of the RobCutt-II are the parameters of propagating waves on bilateral fins, including the left fin frequency, the right fin frequency, the amplitude of waves and the phase difference, which are denoted by F_L, F_R, A, ψ. There is no standard technique for the quantitative analysis of hydrodynamics of the fin propulsion. The limitations of some numerical analysis methods such as finite element method include modelling difficulty, huge computation, and weak real-time performance. To address this challenging problem, fuzzy logic model is proposed to build the nonlinear relationship between the propulsive force/torque and the control parameters of the undulatory fins of the RobCutt-II. The detailed description of the parameter mapping based on fuzzy inference has been given in [14]. Thus, it is omitted.

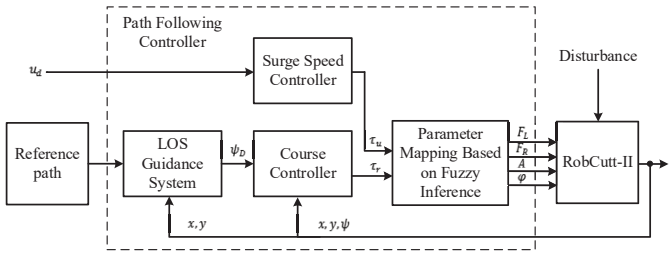

Fig. 3. Block-diagram of the path following controller.

A. LOS Guidance System

As the core component of path following, a LOS guidance system is implemented to accomplish motion planning of the RobCutt-II. The notations of the LOS guidance system are depicted in Fig. 4:

1) $p(x, y)$ and ψ are the real-time position and the course angle of the RobCutt-II, respectively.
2) γ is the radius of the virtual ball associated with the RobCutt-II.
3) ψ_d is the target course angle.
4) $p_{los}(x_d, y_d)$ defines the foresight point.
5) p'_{los} represents the other intersection point.

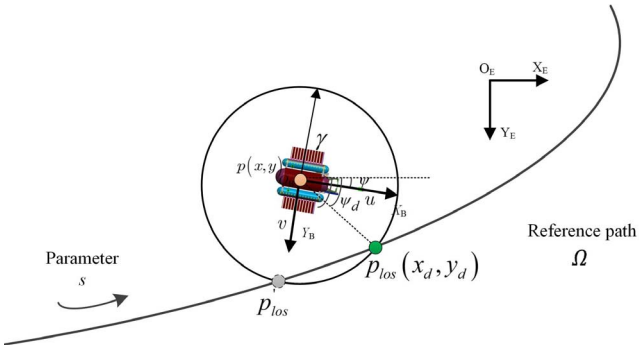

Fig. 4. Modeling of the LOS guidance system.

The LOS guidance system is designed to give the foresight point p_{los} the RobCutt-II needs to track currently in real time based on reference path and position feedback. Fig. 4 shows that the foresight point is located somewhere on the reference path Ω. Specifically, assume that there is a virtual ball, whose center is located in the barycenter of the RobCutt-II and the radius is γ, associated with the RobCutt-II. If the virtual ball intersects the reference path, the intersection point further forward along the path is served as the foresight point. Otherwise, the point, which is both on the reference path and closest to the virtual ball, is chosen as the foresight point. It should be noted that the foresight point is related to the current position of the RobCutt-II. That is, the foresight point is changing along with the motion of the RobCutt-II. Then the target course is determined according to the foresight point.

B. Course Controller

Based on the model (1) of the RobCutt-II, the dynamic equation of orientation can be rewritten as

$$\begin{cases} \dot{\psi} = r \\ \dot{r} = f_\psi(\nu, \tau_d, t) + b_\psi \tau_r \end{cases} \tag{4}$$

where $f_\psi(\nu, \tau_d, t) = -\frac{d_{32}}{m_{33}}v - \frac{d_{33}}{m_{33}}r + \frac{m_{11}-m_{22}}{m_{33}}uv - \frac{m_{23}}{m_{33}}ur - \frac{m_{23}}{m_{33}}\dot{v} + \frac{1}{m_{33}}\tau_{dr}$ is a multivariable function of system states, external disturbances and time, $b_\psi = \frac{1}{m_{33}}$ denotes the control gain. In order to force the RobCutt-II to track the target course angle ψ_d in the presence of disturbances, a course controller is designed based on ADRC technique as shown in Fig. 5.

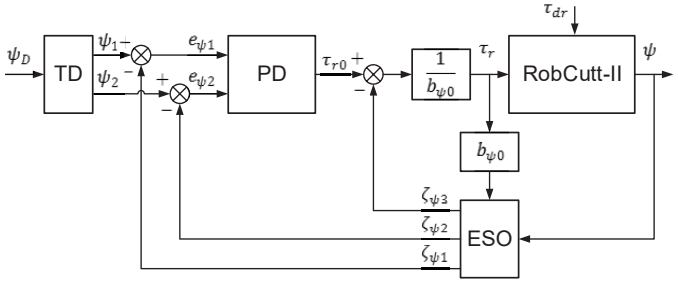

Fig. 5. Block-diagram of the course controller. ψ_d is the target course angle; ψ is the actual course angle of the RobCutt-I; $\tau_{dr}(t)$ represents the external disturbance acted on the course dynamics; $b_{\psi 0}$ is the estimation of control gain, that is, $b_{\psi 0} \approx b_\psi$.

In particular, tracking differentiator (TD) is used to obtain the differential signal and the tracking signal of the setpoint. An extended state observer (ESO) provides an estimate of the internal dynamics of the RobCutt-II and the external disturbances which include the environmental disturbances and the unknown measurement error based on control signal τ_r and system outputs ψ in real time. Once the observer is designed and well tuned, its outputs $\zeta_{\psi 1}$, $\zeta_{\psi 2}$ will track ψ, $\dot{\psi}$ and $\zeta_{\psi 3} \approx f_\psi(\cdot) + (b_\psi - b_{\psi 0})\tau_r$, where $b_{\psi 0}$ denotes the estimation of the control gain of (4). By canceling the effect of f_ψ using $\zeta_{\psi 3}$, the ADRC actively compensates for f_ψ in real time. The ADRC control law for plant (4) is given by

$$\tau_r = \frac{\tau_{r0} - \zeta_{\psi 3}}{b_{\psi 0}} \tag{5}$$

where τ_{r0} will be specified later. By reporting the control signal given by (5) into the control input of plant (4), the plant (4) is simplified as

$$\ddot{\psi} \approx \tau_{r0}. \tag{6}$$

Notice that the plant (4) is reduced to a double integrator. Then, a proportional-derivative (PD) controller is sufficient to control it

$$\tau_{r0} = k_{\psi p} e_{\psi 1} + k_{\psi d} e_{\psi 2} \tag{7}$$

where $k_{\psi p}$ and $k_{\psi d}$ are the proportional gain and derivative gain respectively, $e_{\psi 1} = \psi_1 - \zeta_{\psi_1}$ and $e_{\psi 2} = \psi_2 - \zeta_{\psi_2}$ are states error, ψ_1 is the tracking signal of ψ_D and ψ_2 is the differential signal of ψ_1 subject to the acceleration limit of δ_ψ. The surge speed controller is also designed based on ADRC, which is similar to the one for course control, it is omitted here. The readers may refer to [17] for more details about the mechanism of the ADRC.

IV. SIMULATIONS AND EXPERIMENTAL RESULTS

A. Simulations

To illustrate the performance of the proposed path following method, simulations are carried out with the model shown in Section II. The model parameters used in the simulations are $m_{11} = 57.5$, $m_{22} = 61.3$, $m_{23} = 1.86$, $m_{33} = 1.15$, $d_{11} = 53$, $d_{22} = 58$, $d_{23} = 1.5$, $d_{32} = 1.5$, $d_{33} = 3.1$. Specifically, a typical case to follow a circle is studied. The center and radius of the circle are $(2\,\mathrm{m}, 1.5\,\mathrm{m})$ and $1.1\,\mathrm{m}$, respectively. A full circle is considered, namely, the arc length along the path $s = 2\pi R_c$. The RobCutt-II starts at posture $(0.8\,\mathrm{m}, 1.5\,\mathrm{m}, 0\,\mathrm{rad})$ and the initial velocity is zero. The desired surge speed $u_d = 0.1\,\mathrm{m/s}$. The parameter setting of the path following controller is shown in Table I.

TABLE I
CONTROLLER PARAMETER

h_ψ	δ_ψ	$h_{\psi 0}$	$\omega_{o\psi}$	$b_{\psi 0}$	$k_{\psi p}$	$k_{\psi d}$	γ
0.05	0.3	0.02	1.5	0.8696	25.0	9.0	0.4
h_u	δ_u	h_{u0}	ω_{ou}	b_{u0}	k_{up}	c_0	c_1
0.05	1.5	0.02	2	0.0174	4	2.0	1.5

To reflect the disturbance rejection performance of the controller, zero mean uniform random noises are incorporated into the surge, sway, and yaw dynamics of the RobCutt-II in $20 - 40\,\mathrm{s}$ simulation time. In addition, a constant ocean current disturbance, which is unknown from the point of view of the controller, with intensity $V_c = 0.03\,\mathrm{m/s}$ and direction $\phi_c = \frac{33}{18}\,\mathrm{rad}$ is also added to the controllers dynamic model.

The simulation results based on these conditions are given in Fig. 6-9. Notice that the results of the proportional-integral-differential (PID) controller are shown as the baseline performance in this study and the PID gains were manually tuned for satisfactory performance. Fig. 6 shows the desired path and the actual trajectory of the RobCutt-II. The time evolution of the cross-track errors in simulations are shown in Fig. 7. It is observed that the RobCutt-II converges

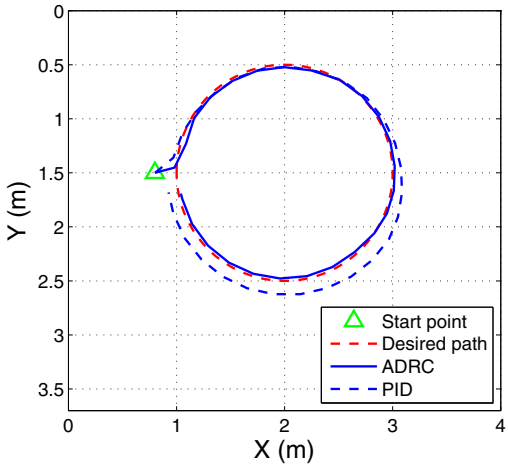

Fig. 6. Simulation trajectory of the RobCutt-II for path following control

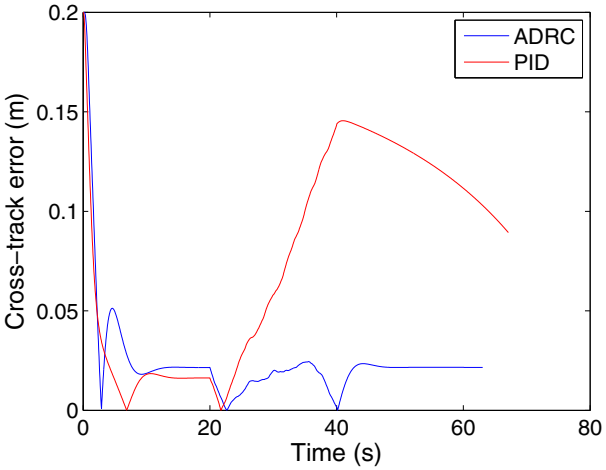

Fig. 7. Time evolution of the cross-track errors

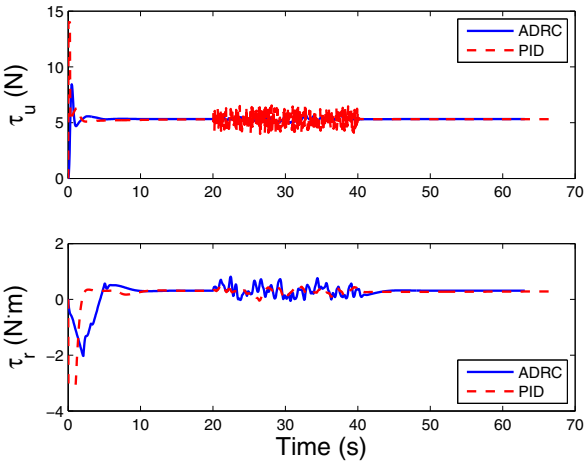

Fig. 8. Time evolution of the vehicle-fixed propulsion force and moment

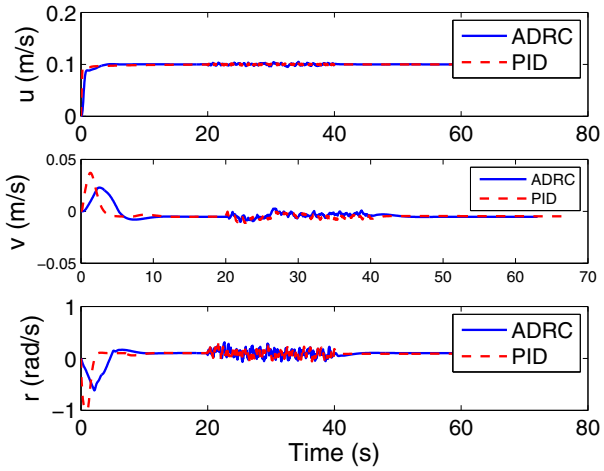

Fig. 9. Time evolution of the body-fixed velocities

to the circle and moves along the desired path by the path following controller based on ADRC, which is effective in reducing the effect of the external disturbance as expected. While PID controller shows large errors around the 20 s when the additional disturbance was applied. Fig. 8 shows the time evolution of the vehicle-fixed propulsive force and moment. Compared with the results of PID, more satisfactory performance can be obtain by the ADRC controller whose jitter amplitude is smaller. Moreover, all control inputs are bounded. Fig. 9 shows the time evolution of the body-fixed velocity. The surge speed shows a fast response without overshoot and maintains at the speed assignment while the velocities in sway and yaw are convergent during the path following.

B. Experimental Results

In order to further evaluate the control system of the RobCutt-II, the experiments of path following are performed in an indoor pool with dimensions of 5 m × 4 m × 1.1 m (length × width × depth). The real-time position and orientation of the RobCutt-II for closed-loop feedback can be obtained based on the global visual tracking system.

TABLE II
CONTROLLER PARAMETER

h_ψ	δ_ψ	$h_{\psi 0}$	$\omega_{o\psi}$	$b_{\psi 0}$	$k_{\psi p}$	$k_{\psi d}$	γ
0.05	0.08	0.02	5	0.25	9	6	0.4
h_u	δ_u	h_{u0}	ω_{ou}	b_{u0}	k_{up}	c_0	c_1
0.05	0.01	0.02	3	0.02	16	1.0	0.95

The center of the desired circle path is $(2.3\,\mathrm{m}, 2\,\mathrm{m})$ and the radius is the same as that of simulation. While the initial states of the RobCutt-II are $(x_0, y_0, \psi_0) = (0.607\,\mathrm{m}, 2.148\,\mathrm{m}, 5.989\,\mathrm{rad})$ and $(u_0, v_0, r_0) = (0.013\,\mathrm{m/s}, 0.012\,\mathrm{m/s}, -0.020\,\mathrm{rad/s})$. Table II tabulates the parameter setting of the path following controller. Notice that the controller parameters of the path following experiment are slightly different from than the simulation settings, possibly due to model uncertainty and strong coupling of the propulsive force and moment of the RobCutt-II.

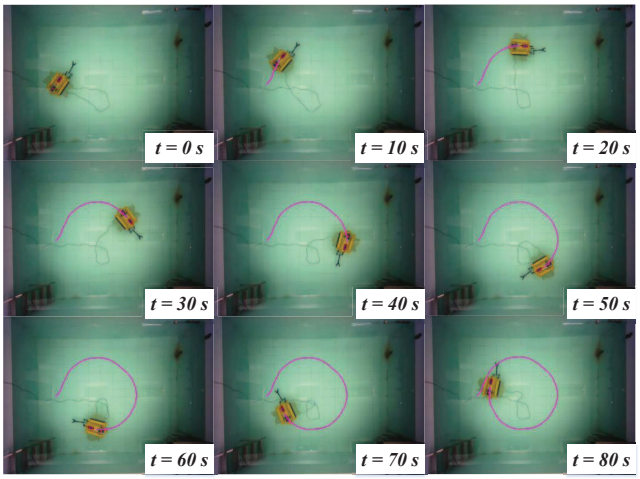

Fig. 10. Consecutive snapshots of path following experiment

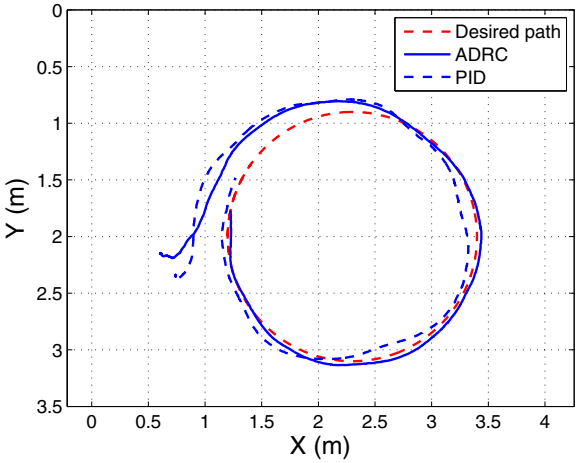

Fig. 11. Trajectory of the RobCutt-II for path following control

It should be mentioned that the indoor pool is not large enough to remove the effects of the reflective waves at present, such that the RobCutt-II is subjecting to external disturbances when it swims in the pool. Fig. 10-12 show the experimental results of the path following. Consecutive snapshots of path following experiment are given in Fig. 10, where the pink curve indicates the trajectory of the RobCutt-II. Analogously, we evaluate the proposed method and the typical PID method. The experimental results are shown in Fig. 11-12. It is observed that two kinds of methods both catch up and follow the desired path. However, the ADRC controller can reach a quicker convergence to the desired path. Furthermore, compared with PID method, the ADRC has a smaller tracking error. Specifically, the maximum cross-track error of the ADRC method after the RobCutt-II converges to the desired path is 0.029 m, while the maximum tracking error of PID is 0.121 m. Therefore, the proposed

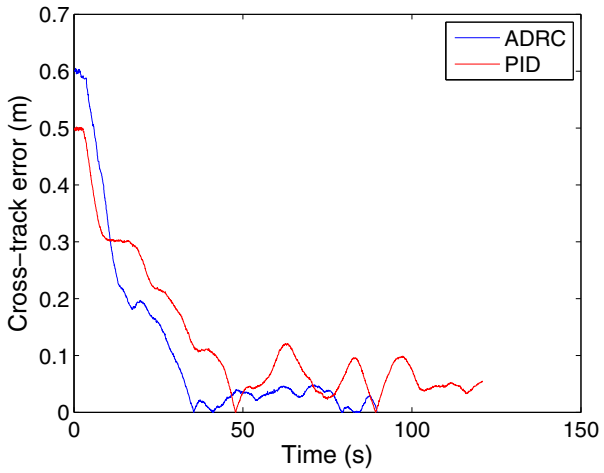

Fig. 12. Time evolution of the cross-track errors

controller is more accurate and effective for path following of the RobCutt-II.

V. CONCLUSIONS AND FUTURE WORK

In this paper, we have proposed a control law for path following of the RobCutt-II, which was designed to imitate the unique propulsion mode of the cuttlefish. A closed-loop control law integrating LOS guidance system and ADR-C technique have been presented for the RobCutt-II path following control. The experimental results show that the BUV is able to autonomously follow reference path in the underwater space. Moreover, compared with traditional PID method, the proposed method reduces the cross-track error with a more satisfactory path following result. This would allow biomimetic underwater vehicles to conduct more accurate and efficient movements and underwater operations than what they were previously capable of.

Future research will concentrate on the 3-D path following control and the hovering control.

VI. ACKNOWLEDGMENTS

This work was supported in part by the National Natural Science Foundation of China under Grant 61233014, 61333016, 51175496, in part by the Foundation for Innovative Research Groups of the National Natural Science Foundation of China under Grant 61421004, and in part by the Beijing Natural Science Foundation under Grant 3141002.

REFERENCES

[1] D. Blidberg, "The development of autonomous underwater vehicles (AUV); a brief summary," in *Proceedings of the 2001 International Conference on Robotics and Automation*, Seoul, South Korea, May 2001.

[2] B. Peter, R. Ratnaweera, W. Fischer, C. Pradalier, R. Siegwart, "Design and evaluation of a fin-based underwater propulsion system," in *Proceedings of the 2011 IEEE International Conference on Robotics and Automation*, Alaska, USA, May 2010, pp. 3751-3756.

[3] M. Sfakiotakis, D. Lane, and B. Davies, "An experimental undulating-fin device using the parallel bellows actuator," in *Proceedings of the 2001 International Conference on Robotics and Automation*, Seoul, South Korea, May 2001, pp. 2356-2362.

[4] R. Torres, O. Curet, G. Lauder, and M. MacIver, "Kinematics of the ribbon fin in hovering and swimming of the electric ghost knifefish," *Journal of Experimental Biology*, vol. 216, no. 5, pp. 823-834, 2013.

[5] M. Rahman, S. Sugimori, H. Miki, R. Yamamoto, Y. Sanada, and Y. Toda, "Braking performance of a biomimetic squid-like underwater robot," *Journal of Bionic Engineering*, vol. 10, no. 3, pp. 265-273, 2013.

[6] K. Do, Z. Jiang, and J. Pan, "Robust adaptive path following of underactuated ships," *Automatica*, vol. 40, no. 6, pp. 929-944, 2004.

[7] A. Aguiar and J. Hespanha, "Trajectory-tracking and path-following of underactuated autonomous vehicles with parametric modeling uncertainty," *IEEE Transactions on Automatic Control*, vol. 52, no. 8, pp. 1362-1379, 2007.

[8] M. Breivik and T. Fossen, "Path following of straight lines and circles for marine surface vessels," in *Proceedings of the 2004 IFAC Conference on Control Applications in Marine Systems*, Ancona, Italy, 2004, pp. 65-70.

[9] E. Fredriksen and K. Pettersen, "Global κ-exponential way-point maneuvering of ships: Theory and experiments," *Automatica*, vol. 42, no. 4, pp. 677-687, 2006.

[10] J. Han, "From PID to active disturbance rejection control," *IEEE Transactions on Industrial Electronics*, vol. 56, no. 3, pp. 900-906, 2009.

[11] Z. Gao, "Scaling and bandwidth-parameterization based controller tuning," in *Proceedings of the 2003 American Control Conference*, New York, USA, 2003, pp. 4989-4996.

[12] Y. Wang, S. Wang, Q. Wei, M. Tan, C. Zhou, and J. Yu, "Development of an underwater manipulator and its free-floating autonomous operation," *IEEE/ASME Transactions on Mechatronics*, vol. 21, no. 2, pp. 815-824, 2016.

[13] R. Wang and S. Wang, "Design and implementation of a biomimetic underwater propeller with a undulating long fin," *Journal of Huazhong University of Science and Technology (Nature Science Edition)*, vol. 43, no. s1, pp. 408-411, 2015.

[14] R. Wang, S. Wang, and Y. Wang, "A hybrid heading control scheme for a biomimetic underwater vehicle," in *Proceedings of the 26th International Ocean and Polar Engineering Conference*, Rhodes, Greece, June 2016, pp. 619-625.

[15] Q. Wei, S. Wang, Y. Wang, C. Zhou, and M. Tan, "Course and depth control for a biomimetic underwater vehicle - RobCutt-I," *International Journal of Offshore and Polar Engineering*, vol. 25, no. 2, pp. 81-87, 2015.

[16] T. Fossen, "Guidance and control of ocean vehicles," New York: Wiley, 1994.

[17] J. Han, "Active disturbance rejection control technique-the technique for estimating and compensating the uncertainties," Beijing: National Defense Industry Press, 2008.